Development of fluid flow evaluation system utilizing time-resolved PIV
（高時間分解PIVを用いた流動評価法の開発 ）

ERKAN NEJDET (エルカン　ネジェット)

1. Introduction

With a high speed camera and a high repetition laser, velocity measurements can be performed at high-temporal and high-spatial resolutions, e.g., 1000x1000 pixels spatial resolution at 5000 Hz. Although huge amount of data, e.g., 5GB per 1 second, can be obtained, the extracted information remains have been limited to some statistical information, i.e., turbulence intensity, power spectrum and so on (Natrajan *et al* 2007, Wernet 2000, Son *et al* 2001 etc.). The development of advanced algorithms and analysis methods are still a necessity for the extraction of the advanced information from the huge amount of TR-PIV data to comprehend the dynamics of fluids.

In this study, three new techniques will be proposed to extract the improved information from the huge amount of TR-PIV data. These techniques are the extraction of fluctuation transfer velocity, out-of-plane velocity extraction for the micro TR-PIV and two kinds of vector extraction from the overlapped micro TR-PIV images. With these new techniques, the measurable information by the TR-PIV will be greatly extended.

2. Fluctuation transfer in turbulent flow

2.1. Background

The spatio-temporal velocity correlation analysis was used for measuring the large-scale structure transfer velocities of a two-dimensional backward-facing step flow utilizing Laser Doppler Velocimetry (LDV) by Furuichi *et al* (2004).

2.2. Experimental setup

Figure 2.1 illustrate the schematic of the target area. A high-speed Photron camera and a Nd:YLF double-pulse laser were used. For this experiment frame straddling technique was utilized, the double pulse interval is arranged as 2 μs and 10 μs. The flow channel has a 10 mm × 10 mm cross-section and a length of 1 m. Two flow cases were studied with Reynolds numbers of 34,000 and 11,000. Nitrogen gas seeded with oil particles using Laskine nozzle.

2.3. Methods

The instantaneous velocity vector maps are calculated using a recursive PIV analysis technique. Figure 2.2 shows sample images and the time-serial relative velocity vector maps. The fluctuation creation on the vortex path occurs with a time delay between two different spatial positions. The measure of the degree of correlation between the two velocity fluctuations is defined as a function of space and time delay in equation (2.1).

$$C(x,y,\tau)_k = \frac{\int_{-\infty}^{\infty} u(x_k,y_k,t)u(x,y,t+\tau)dt}{\sqrt{\int_{-\infty}^{\infty} u(x_k,y_k,t)^2 dt}\sqrt{\int_{-\infty}^{\infty} u(x,y,t+\tau)^2 dt}} \qquad (2.1)$$

$C(x, y, \tau)_k$ is the correlation value. k represents the reference point index and $u(x, y, \tau)$ is the downstream component of the fluctuation velocity. With the delay time of the reference point fixed as zero, the value of τ was changed in the interval of [−2, 2] ms with an increment of 0.1 ms, and the correlations were calculated at every discrete τ values; then the same procedure was applied to all points in the flow field. In the delay time interval of [−2, 2] ms, the correlation value between two points takes a highest value at a particular delay.

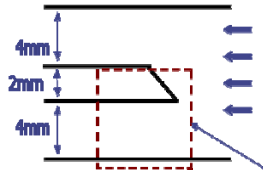

Figure 2.1: Enlarged test section

Correlations and time delay spatial distributions were plotted in figures 2.3 for an arbitrary reference point. Figures 2.3 (*b*) depicts time delay distribution contour map, where reference point location is marked by a black circle. Fluctuating events on the right-hand side occur earlier than the reference point, and fluctuating events on the left-hand side occur after the reference point. Time delay versus *x*-axis graphs (streamwise axes) are plotted as in figure 2.4 for the Reynolds numbers of 11 000 at all chosen reference points.

The inverse of the slope of the delay curve, which is obtained by linear curve fitting in figure 2.4, gives the average transfer velocity of the fluctuations at this point due to equation (2.2).

$$\frac{\partial \tau}{\partial x} = \frac{1}{u_{tr}} \qquad (2.2)$$

2.4. Results and discussions

Two-point velocity correlation was applied, and the normalized fluctuation transfer velocity distribution was obtained in the flow area and depicted in figure 2.5 as a two-dimensional contour map. The green regions in colored maps correspond to approximately half of the average flow velocity in the boundary layer. That result is in good agreement with those from Furuichi *et al* (2004) and Hijikata *et al* (1991). It can be seen that when the average flow velocity is higher, the fluctuation transfer

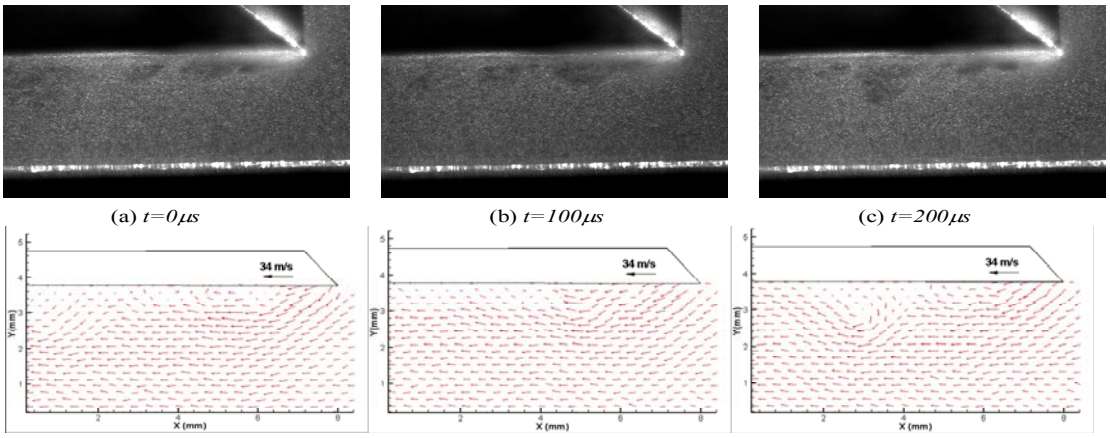

Figure 2.2 Original flow images and instantaneous velocity vectors (Re=34 000).

velocity decreases to smaller values in the boundary layer region.

Spatial and temporal relations of the fluctuating velocities were measured using the time dependent multi-point velocity correlation. That method is not limited to the only two spatial locations in the flow field, but provides full-field fluctuation transfer velocity distribution that differs from the former hot-wire anemometer measurements and that of LDV measurements.

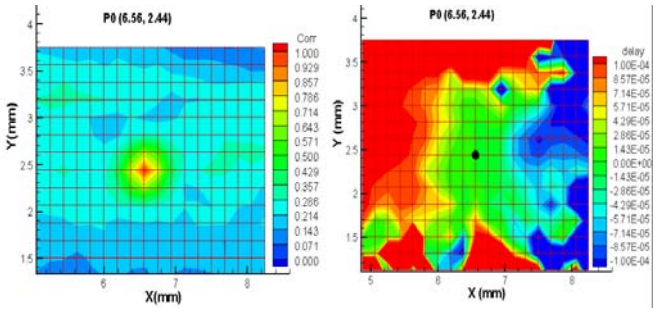

(a) (b)

Figure 2.3: (a) Spatial distribution of correlation values, (b) time delay (in s) distribution of correlation values. (Re=11000)

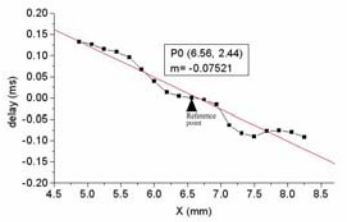

Figure 2.4: Position-time graphs of fluctuation transfers

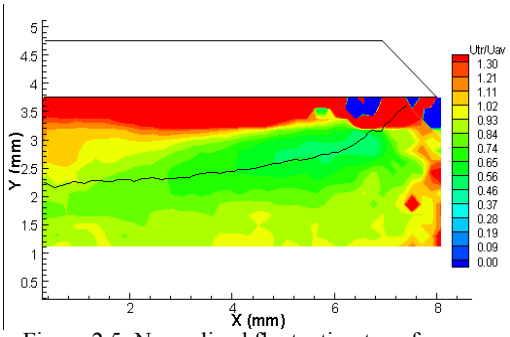

Figure 2.5: Normalized fluctuation transfer velocity distribution. $(u_{tr}(x, y)/U_{av}(x, y))$ (Re = 11 000).

3. Development of 3C velocity field measurement in micro-scales using single high speed camera

3.1. Background

The small working distances associated with microfluidic devices and microscopes provide limited optical access and small spaces to set up experimental apparatus like two cameras to determine the three-component (3C) velocity field.

In this section, simulation of a new 3C velocity measurement technique based on the PIV and performing the correlation peak height tracking inside the small ensembles of the dynamic PIV images in the bounded time intervals will be investigated.

3.2. Synthetic images generation

Several sets of synthetic micro TR-PIV images having different out-of-plane velocities are generated. Every set composed of 12 time sequential images, which all have the same uniform out-of-plane and in-plane velocity in one set, with 512x512 pixels in size. Particle locations are defined randomly within an arbitrary measurement volume. Particle diameters and intensity distributions are defined as proposed by Olsen *et al* (2000).

Synthetic images consisting of 1μm diameter particles were generated as visualized from an optical system

having M = 40, NA=0.8. The depth of field δz of the optical system would be ~7.1 μm.

3.3. PIV analysis and correlation peak tracking

Evaluation procedure composed of two essential parts. First one is instantaneous in-plane velocity measurement using recursive PIV analysis technique, the other one is the CC peak value tracking in the time sequential images with respect to a reference image.

Instantaneous velocity vector maps are calculated using window deformation iterative multi grid image distortion interrogation algorithm (Scarano 2002). Description of the cross-correlation function described initially as;

$$C_{f,g}(m,n)=\frac{\sum_{i=0}^{M}\sum_{j=0}^{N}[f(i,j)-\mu_f][g(i-m,j-n)-\mu_g(m,n)]}{\sqrt{\sigma_f(m,n)}\sqrt{\sigma_g(m,n)}} \quad (3.1)$$

$$\sigma_f(m,n)=\sum_{i=0}^{M}\sum_{j=0}^{N}[f(i,j)-\mu_f]^2$$

$$\sigma_g(m,n)=\sum_{i=0}^{M}\sum_{j=0}^{N}[g(i-m,j-n)-\mu_g(m,n)]^2$$

$C_{f,g}(m,n)$ is the correlation value at a point m, n in search window between the first image's intensity distribution f and the second image's intensity distribution g over the interrogation window. μ is the average intensity of the interrogation window. The particle image displacement is obtained as the distance of the maximum from the origin of the correlation map. When iterative PIV evaluation is applied, the particle displacements evaluated from CC are used to obtain a displacement predictor field at each pixel position. The displacement predictor is used to deform the original images to eliminate the in-plane displacements and make them virtually similar. These regenerated images are re-correlated with each other with a reduced interrogation window size and the displacement results are added to the previous displacements.

When the above evaluation procedure is performed by taking one median image as a reference image, correlate it with the forward and backward images by shifting in the time domain, it would be seen that CC peak height is changing with respect to the time.

Maximum value of $C_{k,\,k+\tau}$,which is defined in Equation 3.1, for an interrogation area is calculated for $\forall\tau\in[-5,5]$ at an arbitrary spatial position, and then alteration of $C_{k,\,k+\tau}$ versus the discrete time shift value of τ is plotted in Figure 3.1. CC value changes almost linearly. In the next section, these correlation curves including both left and right side are going to be fitted to a linear curve with a particular deviation i.e. $EPS=\sum_i[y_i-(ax_i+b)]^2$, then inclination of that curve would give us the rate of change of the CC peak height with respect to the time. That rate and particle's out-of-plane velocity would be associated.

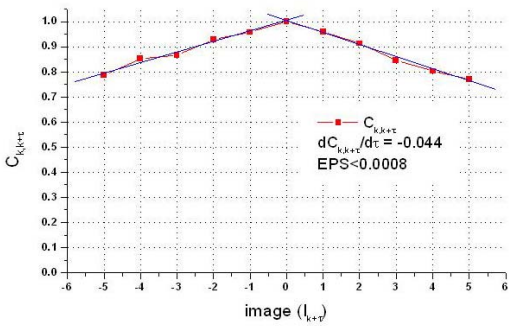

Figure 3.1: Cross-correlation peak height change versus image number at an arbitrary spatial

3.4. Results and Discussions

Above method is repeated for all synthetic image sets which have different out-of-plane velocities. And finally, evolution of time gradient of CC peak height with respect to the out-of-plane velocity is plotted in Figure 3.2. Horizontal axis is taken as the ratio of the out-of-plane velocity to the depth of field of the simulated optical system. The CC gradient values were chosen for relatively well linear fitted spatial locations.

Rate of decrease in CC peak height is linearly dependent to the out-of-plane velocity. It can be detected with a chi-square (*EPS*) less then 0.0008 if the out-of-plane displacement is less than around 10% of depth of field of the optical system.

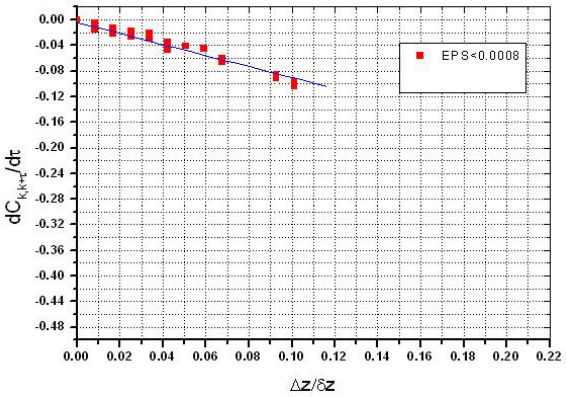

Figure 3.2: Cross-correlation gradient evolution with respect to Δz/δz.

4. Measurement of complex flow fields in micro-scales

The mixing is achieved in chaotic mixers (Stroock et al 2002) with mainly transverse velocity components of the flow that causes sensors to capture complicated PIV images which have particle images moving in the different directions with different velocities on the same image plain.

In this section, two kinds of velocity extraction method for the complex flows in the micro-channels having grooved inner surfaces is investigated by making use of the huge amount of time-resolved PIV data.

4.1. Experimental setup and Methodology

Flow images were recorded via an epiflourescence microscope with a water-immersion objective lens (M=40, NA=0.8). A schematic view of the rectangular micro channel with obliquely oriented ridges is shown in Figure 4.1.

4.2. Method of analysis

If depth of the bottom groove is 5-10 μm, it is almost equivalent to the thickness of the measurement plane of the micro PIV system. Therefore, measurement of the velocity field near the groove is very difficult due to the existence of the tracing particles which have different velocities in the same measurement volume that they are placed on the same image plane (Figure 4.1).

Unlike the classical PIV images, there are two different velocity vector fields in our measurement plane. Dynamic ensemble correlation method (Equation 4.1) is proposed to extract these velocity vectors.

$$R_\tau(m,n) = \frac{1}{Z}\sum_{k=1}^{Z} C_{(k,k+\tau)}(m,n) \quad (4.1)$$

$C_{(k,\ k+\tau)}$ (m,n) defined in Equation 3.1 is the correlation value. τ is the time interval i.e. skipping image number. R_τ is the final average cross-correlation value at a point (m, n). A contour map of the ensemble correlation function $R_\tau(m,n)$ for $\tau=25$,$Z=3000$ value in an interrogation area is plotted in Figure 4.2.

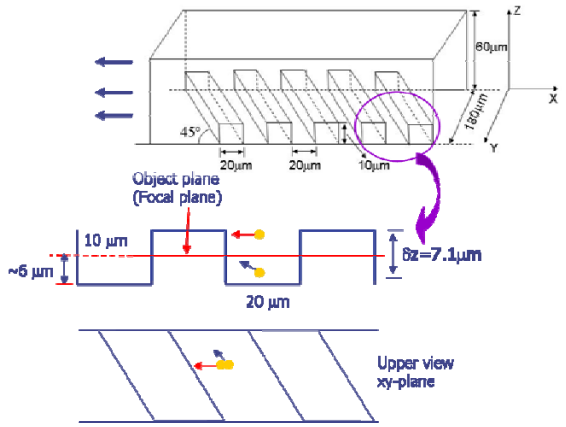

Figure 4.1 Target flow area near to the grooves.

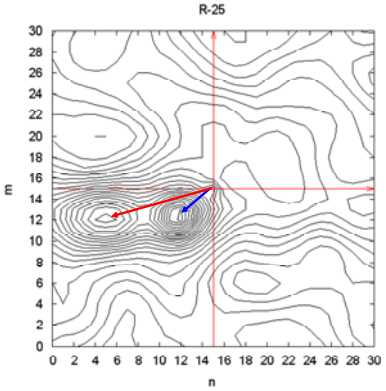

Figure 4.2 Dynamic ensemble correlation maps. A sample interrogation window on the groove.

4.3 Results

Water inside the channel flows with a Reynolds number of 0.32 and average velocity of 1.5 mm/s in laminar mode. Overlapped velocity vectors are presented in Figure 4.3. *Fast* describes the velocity vectors obtained from the particles moving above the grooves and *Slow* describes the velocity vectors obtained from the particles moving inside of the grooves. Because of the high reflections and background noise, overlapped velocity vectors could not be detected in every grid positions. Also 1 μm diameter fluorescent flow tracing particles were used. That size is quite big as much as not to be able to detect chaotic velocity fluctuations in such a small length scales.

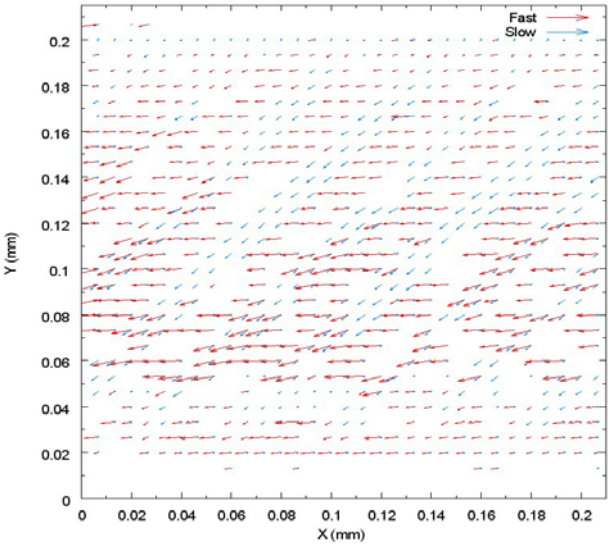

Figure 4.3 Velocity vector map.

5. Conclusion

Three evaluation methods have been proposed in order to extract the advanced information from the huge amount of Dynamic-PIV data. These methods make use of the huge amount of temporal data for the evaluation of the fluid flow covering wide dynamic range and spatial range i.e. laminar flow inside the micro-channels and high-speed turbulent flow in macro scales.

It is demonstrated that high-time resolved information acquired by dynamic-PIV is not used only for temporally fine resolved instantaneous velocity vector field realizations, but also extraction of advanced information including 3C velocity, full-field turbulent large structure transfer velocity and two different overlapped vector fields from the same image of micro-scale chaotic flow.

6. References

Furuichi N *et al* (2004), *Exp. Fluids* 36 274–81

Hijikata K *et al* (1991), *ASME-FED Exp. Num. Flow Vis.*128:61–8

Natrajan V.K. *et al* (2007) *Microfluid Nanofluid* 3: 89-100.

Olsen M G, Adrian R J (2000), *Exp. Fluids* [Suppl.]:S166-174.

Scarano F (2002), *Meas. Sci. Technol.* 13: R1-R19

Stroock A. D. et al. (2002), *Science* 295: 647-651.
Son SY, Kihm KD (2001) *Exp. Fluids* 30 (5): 537-550
Wernet M.P. (2000) Optics and Laser Technol. 32: 7-8